

# Predictive powers of chiral perturbation theory in Compton scattering off protons

Vadim Lensky<sup>1,2,\*</sup> and Vladimir Pascalutsa<sup>1,3</sup>

<sup>1</sup>*European Centre for Theoretical Studies in Nuclear Physics and Related Areas (ECT\*),  
Villa Tambosi, Villazzano (Trento), I-38050 TN, Italy*

<sup>2</sup>*Institute for Theoretical and Experimental Physics, 117218 Moscow, Russia<sup>†</sup>*

<sup>3</sup>*Institut für Kernphysik, Johannes Gutenberg Universität, Mainz D-55099, Germany*

(Dated: September 12, 2018)

## Abstract

We study low-energy nucleon Compton scattering in the framework of baryon chiral perturbation theory (B $\chi$ PT) with pion, nucleon, and  $\Delta(1232)$  degrees of freedom, up to and including the next-to-next-to-leading order (NNLO). We include the effects of order  $p^2$ ,  $p^3$  and  $p^4/\Delta$ , with  $\Delta \approx 300$  MeV the  $\Delta$ -resonance excitation energy. These are all “predictive” powers in the sense that no unknown low-energy constants enter until at least one order higher (i.e.  $p^4$ ). Estimating the theoretical uncertainty on the basis of natural size for  $p^4$  effects, we find that uncertainty of such a NNLO result is comparable to the uncertainty of the present experimental data for low-energy Compton scattering. We find an excellent agreement with the experimental cross section data up to at least the pion-production threshold. Nevertheless, for the proton’s magnetic polarizability we obtain a value of  $(4.0 \pm 0.7) \times 10^{-4} \text{ fm}^3$ , in significant disagreement with the current PDG value. Unlike the previous  $\chi$ PT studies of Compton scattering, we perform the calculations in a manifestly Lorentz-covariant fashion, refraining from the heavy-baryon (HB) expansion. The difference between the lowest order HB $\chi$ PT and B $\chi$ PT results for polarizabilities is found to be appreciable. We discuss the chiral behavior of proton polarizabilities in both HB $\chi$ PT and B $\chi$ PT with the hope to confront it with lattice QCD calculations in a near future. In studying some of the polarized observables, we identify the regime where their naive low-energy expansion begins to break down, thus addressing the forthcoming precision measurements at the HIGS facility.

PACS numbers: 13.60.Fz - Elastic and Compton scattering, 14.20.Dh - Protons and neutrons, 25.20.Dc - Photon absorption and scattering, 11.55.Hx Sum rules

---

<sup>†</sup> On leave of absence.

\*Electronic address: [lensky@ect.it](mailto:lensky@ect.it)

<b>Contents</b>	
<b>I. Introduction</b>	2
<b>II. Chiral Lagrangians and power counting</b>	4
<b>III. Compton amplitude at NNLO</b>	6
A. Graphs and the nucleon field redefinition	6
B. Renormalization	10
C. Consistency with forward-scattering sum rules	11
D. Error due to $\mathcal{O}(p^4)$ effects	12
<b>IV. Proton polarizabilities</b>	13
<b>V. Results for cross sections</b>	15
A. Unpolarized	15
B. Polarized	18
<b>VI. Conclusion</b>	19
<b>Acknowledgments</b>	20
<b>A. Chiral loop contributions to polarizabilities</b>	20
1. Nucleon Loops	20
2. Delta Loops	21
<b>B. Low-energy expansion for cross sections</b>	21
<b>References</b>	22

## I. INTRODUCTION

Compton scattering off nucleons has a long and exciting history, see Refs [1–3] for recent reviews. The 90’s witnessed a breakthrough in experimental techniques which led to a series of precision measurements of Compton scattering [4–9] with the aim to determine the nucleon *polarizabilities* [10, 11].

Many theoretical approaches have been tried in the description of nucleon polarizabilities and low-energy Compton scattering. The more prominent examples include dispersion relations [12–18], effective-Lagrangian models [19–22], constituent quark model [23], and chiral-soliton type of models [24–28]. There has been as well a significant recent progress in approaching the subject from first principles—lattice QCD (lQCD). The present lQCD studies are based on the external electromagnetic field method [29, 30], and even though the actual results for the nucleon have been obtained only in quenched approximation, the pion and kaon polarizabilities have been calculated with dynamical quarks [31]. The full-lQCD calculations for the nucleon will hopefully be done in a near future.

In this work we exploit another theoretical approach rooted in QCD, namely, chiral perturbation theory ( $\chi$ PT) [32–35]. The very first  $\chi$ PT calculation of nucleon polarizabilities, published in 1991 by Bernard, Kaiser and Meißner [36], quotes the result shown in the  $\mathcal{O}(p^3)$

column of Table I. In the same column, the numbers in brackets show the result of the so-called heavy-baryon (HB) expansion [38]. Here it means that one additionally expands the full result [36] in powers of  $m_\pi/M_N$ , the ratio of the pion and nucleon masses, and drops all but the leading terms (cf. Appendix A). The  $\mathcal{O}(p^3)$  HB $\chi$ PT result thus corresponds to the static nucleon approximation. The relativistic effects are systematically included in HB $\chi$ PT at higher orders, but nonetheless even leading order HB $\chi$ PT result is widely considered to be more consistent than the B $\chi$ PT (i.e., fully relativistic) one. The reason for that is that the full relativistic evaluation of the chiral loops may yield contributions which are of lower order than is given by the power-counting argument. This “pathology”, however, does not arise in the case of polarizabilities at  $\mathcal{O}(p^3)$ , so as far as power counting is concerned, the B $\chi$ PT result is as good here as the one of HB $\chi$ PT. But even more generally, chiral symmetry ensures that the power-counting violating terms to be always accompanied by low-energy constants (LECs), hence they can simply be removed in the course of renormalization of those LECs [39, 40]. In simpler terms, there is no problem with power counting in B $\chi$ PT.

The present state-of-the-art  $\chi$ PT studies based on pion and nucleon degrees of freedom [41, 42] utilize the HB expansion. They find, however, that despite the very reasonable values for polarizabilities, the  $\mathcal{O}(p^3)$  and even  $\mathcal{O}(p^4)$  results for the Compton-scattering cross sections show significant discrepancy with experimental data starting from energies of about 120 MeV, especially at backward kinematics. The inclusion of the  $\Delta(1232)$ -resonance as an explicit degree of freedom helps to remedy this discrepancy in the cross sections [43, 44]. However, it comes at an expense of a large contribution to the polarizabilities [45]. This  $\Delta$ -contribution is highly unwanted in HB $\chi$ PT, since polarizabilities come out nearly perfect already in the theory without the  $\Delta$  (cf. the numbers in brackets in Table I). There is no natural solution to this problem. One is bound to either omit some of the  $\Delta$  contributions by “demoting” them to higher orders [43], or cancel them by “promoting” some of the low-energy constants (LECs) to lower orders [44].

Such an apparent failure of  $\chi$ PT is sometimes attributed to certain “ $\sigma$ -meson” contributions [46], which  $\chi$ PT misses. Of course, while the  $\sigma$ -meson of the linear sigma model is included in  $\chi$ PT, the contribution from the  $f_0(600)$  is not, but it is doubtful that the  $f_0$  can explain it; its two-photon coupling is too small. Alternatively, studies based on dispersion relations suggest that some essentially relativistic effects, discarded in HB $\chi$ PT as being higher order, are in fact important because of the proximity of cuts in both pion mass and energy [47–49].

In our present study we verify the latter scenario and perform the calculations in a manifestly Lorentz-covariant fashion, refraining from the use of the heavy-baryon formalism. The HB $\chi$ PT results can then be recovered by simply expanding in powers of pion mass over the baryon mass,  $m_\pi/M_B$ . We thus are coming back to the original (relativistic quantum field theory) ways [36]. The difference with the original work [36] is that we compute the Compton scattering observables, not only the scalar polarizabilities, and that we include the  $\Delta(1232)$  in addition to the pion and nucleon degrees of freedom.

Table I shows the results of both manifest-covariant and HB calculations at all the “predictive” orders, i.e., below  $\mathcal{O}(p^4)$  — the order at which the unknown LECs start to enter. A natural estimate of the  $\mathcal{O}(p^4)$  contribution, given in the corresponding column, can serve as an error bar on the  $\chi$ PT prediction. A detailed discussion of these results can be found in Sect. IV. It can be noted, however, how significant the differences are between the exact and

	B $\chi$ PT (HB $\chi$ PT)			PDG
	$\mathcal{O}(p^3)$	$\mathcal{O}(p^3) + \mathcal{O}(p^4/\Delta)$	$\mathcal{O}(p^4)$ est.	[37]
$\alpha^{(p)}$	6.8 (12.2)	10.8 (20.8)	$\pm 0.7$	$12.0 \pm 0.6$
$\beta^{(p)}$	-1.8 (1.2)	4.0 (14.7)	$\pm 0.7$	$1.9 \pm 0.5$

TABLE I: Predictions of baryon  $\chi$ PT for electric ( $\alpha$ ) and magnetic ( $\beta$ ) polarizabilities of the proton in units of  $10^{-4} \text{ fm}^3$ , compared with the Particle Data Group summary of experimental values.

the HB results. This is of course not the first and only example where B $\chi$ PT and HB $\chi$ PT are in dissent, see e.g., the case of  $\gamma N \rightarrow \Delta$  transition [50, 51], or the baryon magnetic moments in SU(3) [52, 53]. These differences can often be significantly diminished by slight improvements of the HB calculations, such as readjusting the position of the thresholds to have them in the exactly correct place [41]. It is not yet clear, however, how to systematically derive such improvements from the HB formalism itself.

As to why the orders considered here are *predictive*, any chiral power-counting scheme will tell us that the expansion of the Compton amplitude begins at order  $p^2$ , and that  $p^4$  is the order where the first unknown LECs should enter. In between there are  $p^3$  and the  $\Delta$ -excitation effects. The counting for the latter is itself a subject of controversy related to the issue of how to count the  $\Delta$ -nucleon mass difference:  $\Delta = M_\Delta - M_N \approx 300 \text{ MeV}$ . In the hierarchy of chiral symmetry breaking scales,  $\Delta$  is neither as light as the scale of explicit symmetry-breaking,  $m_\pi \sim 150 \text{ MeV}$ , nor as heavy as the scale of spontaneous symmetry-breaking,  $4\pi f_\pi \sim 1 \text{ GeV}$ . We treat  $\Delta$  as an independent light scale with the power-counting rules defined in Sect. II. In any case, the leading  $\Delta$  effects come before  $p^4$ .

To recapitulate, in this work we compute the contributions to Compton amplitude up to, but not including,  $\mathcal{O}(p^4)$  in B $\chi$ PT with  $\Delta$ 's. This is a complete next-to-next-to-leading order (NNLO) calculation which is entirely expressed in terms of only known LECs. The details of these calculations are given in Sect. III. Polarizabilities and their chiral behaviors are discussed in Sect. IV while the results for observables are shown in Sect. V.

Some of these results have recently been reported in a letter [54]. The present paper is more comprehensive and self-contained.

## II. CHIRAL LAGRANGIANS AND POWER COUNTING

The method of constructing the chiral SU(2) Lagrangians with pion and nucleon fields is well known [34, 35, 55], and the inclusion of the  $\Delta$ -isobar fields in a Lorentz-covariant fashion has recently been reviewed [56]. We shall list here only the terms relevant to the present work. The strong-interaction piece is given by

$$\mathcal{L}_\pi^{(2)} = \frac{f^2}{4} \text{tr}(\partial^\mu U \partial_\mu U^\dagger + 2B_0(UM^\dagger + MU^\dagger)), \quad (1a)$$

$$\mathcal{L}_N^{(1)} = \bar{N} (i\not{\partial} - M_N + \not{\psi} + g_A \not{\psi} \gamma_5) N, \quad (1b)$$

$$\mathcal{L}_\Delta^{(1)} = \bar{\Delta}_\mu (i\gamma^{\mu\nu\lambda} \partial_\lambda - M_\Delta \gamma^{\mu\nu}) \Delta_\nu + \frac{h_A}{2M_\Delta} [i\bar{N} T_a \gamma^{\mu\nu\lambda} (\partial_\mu \Delta_\nu) \text{tr}(a_\lambda \tau^a) + \text{H.c.}], \quad (1c)$$

where  $U$  is the SU(2) pion field in the exponential parameterization:  $U = \exp(i\pi^a \tau^a / f)$ ,  $f$  is the pion decay constant in the chiral limit,  $M$  is the mass matrix of light quarks, and  $B_0$

is a proportionality factor that can be related with the value of light quark condensate [34]. In turn,  $N$  denotes the isodoublet Dirac field of the nucleon,  $M_N$  is the nucleon mass, and  $g_A$  is the axial-coupling constant, both taken at their chiral-limit value, and the vector and axial-vector chiral fields above are defined in terms of the pion field,  $\pi^a(x)$ , as

$$v_\mu \equiv \frac{1}{2} \tau^a v_\mu^a(x) = \frac{1}{2i} (u \partial_\mu u^\dagger + u^\dagger \partial_\mu u), \quad (2a)$$

$$a_\mu \equiv \frac{1}{2} \tau^a a_\mu^a(x) = \frac{1}{2i} (u^\dagger \partial_\mu u - u \partial_\mu u^\dagger), \quad (2b)$$

where  $u = \exp(i\pi^a \tau^a / 2f) = U^{1/2}$ . Finally,  $\Delta_\nu$  is the Delta isobar Rarita–Schwinger field with mass  $M_\Delta$ , and  $h_A$  is the  $\pi N \Delta$  coupling constant whose value is fixed to the  $\Delta \rightarrow \pi N$  decay width of 115 MeV. The antisymmetrized products of Dirac matrices in the above equations are defined as:  $\gamma^{\mu\nu} = \frac{1}{2}(\gamma^\mu \gamma^\nu - \gamma^\nu \gamma^\mu)$  and  $\gamma^{\mu\nu\lambda} = \frac{1}{2}(\gamma^{\mu\nu} \gamma^\lambda + \gamma^\lambda \gamma^{\mu\nu})$ . The isospin  $1/2 \rightarrow 3/2$  transition matrix  $T$  is normalized such that  $T^a T^{b\dagger} = \frac{1}{3}(2\delta^{ab} - i\epsilon^{abc} \tau^c)$ .

The electromagnetic interaction is added as usual through the minimal substitution:

$$\partial_\mu N \rightarrow \partial_\mu N - ie A_\mu \frac{1}{2}(1 + \tau_3)N, \quad (3a)$$

$$\partial_\mu \pi^a \rightarrow \partial_\mu \pi^a - e A_\mu \epsilon^{ab3} \pi^b, \quad (3b)$$

where  $A_\mu$  is the photon field. The minimal coupling of the photon to the Delta field gives contributions to Compton scattering which are of higher orders than the ones considered in this work.

There is as well a number of nonminimal terms:

$$\mathcal{L}_N^{(2)} = \frac{e\kappa_{p,n}}{4M_N} \bar{N} \frac{1}{2}(1 \pm \tau_3) \gamma^{\mu\nu} N F_{\mu\nu}, \quad (4a)$$

$$\mathcal{L}_\Delta^{(2)} = \frac{3e}{2M_N(M_N + M_\Delta)} \bar{N} T_3 \left( ig_M \tilde{F}^{\mu\nu} - g_E \gamma_5 F^{\mu\nu} \right) \partial_\mu \Delta_\nu + \text{H.c.}, \quad (4b)$$

$$\mathcal{L}_{\text{WZW}}^{(4)} = -\frac{e^2}{32\pi^2 f} F_{\mu\nu} \tilde{F}^{\mu\nu} \pi_3.$$

Here,  $F^{\mu\nu}$  and  $\tilde{F}^{\mu\nu}$  are the photon field strength tensor and its dual tensor defined as  $F^{\mu\nu} = \partial^\mu A^\nu - \partial^\nu A^\mu$ ,  $\tilde{F}^{\mu\nu} = \frac{1}{2}\epsilon^{\mu\nu\rho\lambda} F_{\rho\lambda}$ ;  $\kappa_p$  ( $\kappa_n$ ) stands for the proton's (neutron's) anomalous magnetic moment;  $g_E$  and  $g_M$  are  $\gamma N \Delta$  electric and magnetic couplings, respectively, which are well known from the analysis of pion-photoproduction  $P_{33}$  multipoles [51]. Here we differ from the strategy adopted in Ref. [43], where, in the absence of any  $\chi$ PT analysis of pion-photoproduction at the time, the values of  $g_E$  and  $g_M$  were fitted to Compton scattering data, with a rather unsatisfactory result. The precise values of all the parameters used in the present work are given in Table II.

Inclusion of the  $\Delta$ -isobar fields in a Lorentz-covariant fashion raises the consistency problems of higher-spin field theory [57–59]. The  $\Delta$ -isobar couplings used here possess the property of invariance under a gauge transformation:  $\Delta_\mu \rightarrow \Delta_\mu + \partial_\mu \epsilon$ , where  $\epsilon$  is an arbitrary spinor field. This ensures the decoupling of unphysical spin-1/2 degrees of freedom and eliminates the consistency problems [60, 61]. It is far less straightforward to reconcile this extra gauge symmetry with other symmetries of the chiral Lagrangian. For recent progress see Refs. [56, 62, 63].

Coming to the power counting, for the pion and nucleon contributions we shall use the usual scheme [35], i.e., a graph with  $V_k$  vertices from  $\mathcal{L}^{(k)}$ ,  $L$  loops,  $N_\pi$  pion and  $N_N$  nucleon

$\mathcal{O}(p^2)$	$\frac{e^2}{4\pi} = \frac{1}{137}, M_N = 938.3 \text{ MeV}, \hbar c = 197 \text{ MeV}\cdot\text{fm}$
$\mathcal{O}(p^3)$	$g_A = 1.267, f_\pi = 92.4 \text{ MeV}, m_\pi = 139 \text{ MeV}, m_{\pi^0} = 136 \text{ MeV}, \kappa_p = 1.79$
$\mathcal{O}(p^4/\Delta)$	$M_\Delta = 1232 \text{ MeV}, h_A = 2.85, g_M = 2.97, g_E = -1.0$
$\mathcal{O}(p^4)$	$\alpha_0, \beta_0 = \pm \frac{e^2}{4\pi M_N^3}$

TABLE II: Parameters (fundamental and low-energy constants) at the order they first appear.

lines is of order  $p^n$  with

$$n = \sum_k kV_k + 4L - 2N_\pi - N_N. \quad (5)$$

In the case of Compton scattering by  $p$  we understand the photon energy or/and the pion mass as compared with  $4\pi f_\pi \sim 1 \text{ GeV}$ .

The graphs with  $\Delta$ s are more tricky because for small  $p$  they go as

$$S_\Delta \sim \frac{1}{p \pm \Delta} \quad (6)$$

rather than simply  $1/p$  as the nucleon propagators. The new scale

$$\Delta = M_\Delta - M_N \simeq 293 \text{ MeV} \quad (7)$$

is neither as light as  $m_\pi$  nor as heavy as  $4\pi f_\pi$ , hence can and will be treated independently. For energies comparable to the pion mass we choose to additionally expand in  $p/\Delta$ , and hence the  $\Delta$  propagator counts as  $1/\Delta$ , while a graph with  $N_\Delta$  internal lines contributes to order

$$p^n \left(\frac{1}{\Delta}\right)^{N_\Delta}. \quad (8)$$

For definiteness, when needed, we count  $\Delta^2$  to be of  $\mathcal{O}(p)$ , i.e., the “ $\delta$  counting” scheme [43].

For the power counting in the region where the energies are of order of  $\Delta$  (the resonance region) see [43, 51]. Hereby we limit ourselves to the low-energy region,

$$p \sim m_\pi \ll \Delta \ll 4\pi f_\pi. \quad (9)$$

### III. COMPTON AMPLITUDE AT NNLO

#### A. Graphs and the nucleon field redefinition

The chiral expansion for the Compton amplitude begins with graph (1) in Fig. 1 and its crossed counterpart. Nominally they both are of  $\mathcal{O}(p)$ , however, together they simply give the Thomson amplitude, which is of  $\mathcal{O}(p^2)$ . We thus refer to  $\mathcal{O}(p^2)$  as the leading order (LO). The other graphs in Fig. 1 contribute to  $\mathcal{O}(p^3)$ , the next-to-leading order (NLO).



FIG. 1: The tree graphs evaluated in this work. Graphs obtained from these by crossing and time reversal are not shown, but are evaluated too. Dots stand for the (leading)  $\gamma NN$  and  $\pi NN$  vertices from  $\mathcal{L}^{(1)}$ , whereas crossed circle denotes the  $\mathcal{L}^{(2)}$  coupling via anomalous magnetic moment. Filled square stands for the WZW-anomaly  $\pi^0\gamma\gamma$  vertex from  $\mathcal{L}^{(4)}$ .

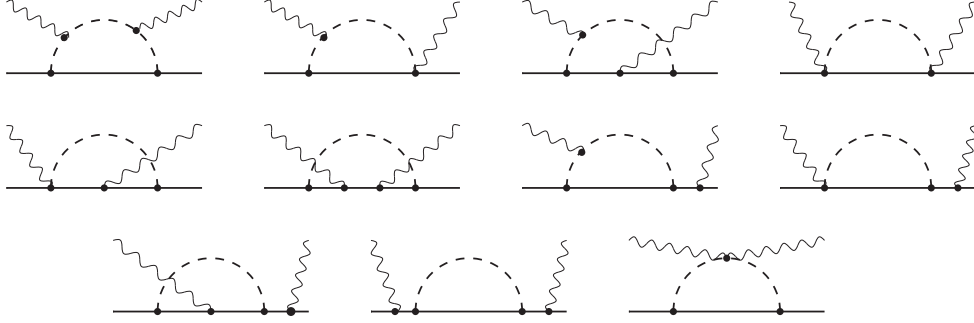


FIG. 2: The one-loop graphs contributing to Compton scattering at  $\mathcal{O}(p^3)$ . Graphs obtained from these by crossing and time reversal are not shown.

At NLO we also have the one-loop contributions shown in Fig. 2, but before evaluating them we make a redefinition of the nucleon field,  $N \rightarrow \xi N$ , where

$$\xi = \exp\left(\frac{ig_A \pi^a \tau^a}{2f} \gamma_5\right). \quad (10)$$

The first-order chiral Lagrangian Eq. (1b) then becomes:<sup>1</sup>

$$\begin{aligned} \mathcal{L}'_N{}^{(1)} &= \bar{N} \xi (i\not{D} - M_N + g_A \not{d} \gamma_5) \xi N \\ &= \bar{N} (i\not{d} - M_N) N + M_N \bar{N} (1 - \xi^2) N \\ &\quad + \bar{N} (\xi i\not{d} \xi - \xi \not{d} \xi + g_A \xi \not{d} \gamma_5 \xi) N. \end{aligned} \quad (11)$$

The two Lagrangians are equivalent, in the sense of equivalence theorem, however, may have drastically different forms when expanded in the pion field. For the one-loop contributions to Compton scattering it is sufficient to expand up to the second order in the pion field:

$$v_\mu = \frac{1}{4f^2} \tau^a \varepsilon^{abc} \pi^b \partial_\mu \pi^c + \mathcal{O}(\pi^3), \quad (12a)$$

$$a_\mu = \frac{1}{2f} \tau^a \partial_\mu \pi^a + \mathcal{O}(\pi^3), \quad (12b)$$

$$\xi = 1 + \frac{ig_A}{2f} \tau^a \pi^a \gamma_5 - \frac{g_A^2}{8f^2} \pi^2 + \mathcal{O}(\pi^3). \quad (12c)$$

<sup>1</sup> In our conventions  $\gamma_5^\dagger = \gamma_5$ , hence  $\xi^\dagger = \exp(-ig\pi^a \tau^a \gamma_5 / 2f_\pi)$ ,  $\xi \xi^\dagger = 1$ . Note also that  $\bar{N} \rightarrow \bar{N} \xi$ , and  $\xi \gamma^\mu \xi = \gamma^\mu$ .

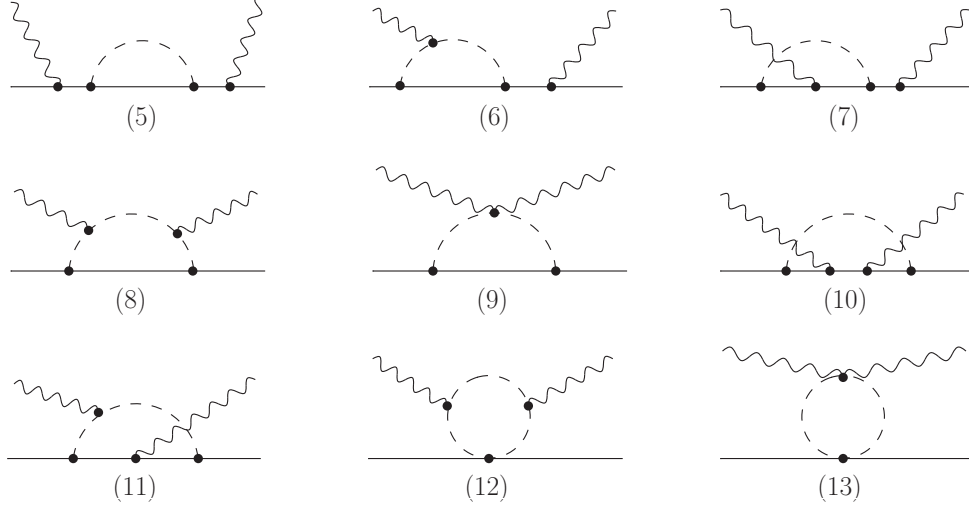


FIG. 3: The NLO loop graphs evaluated in this work. Graphs obtained from these by crossing and time reversal are not shown, but are evaluated too.

The original and the redefined Lagrangians take, respectively, the following form:

$$\begin{aligned} \mathcal{L}_N^{(1)} = \bar{N} & \left( i\not{\partial} - M_N + \frac{g_A}{2f} \tau^a \not{\partial} \pi^a \gamma_5 \right. \\ & \left. - \frac{1}{4f^2} \tau^a \varepsilon^{abc} \pi^b \not{\partial} \pi^c \right) N + \mathcal{O}(\pi^3), \end{aligned} \quad (13)$$

$$\begin{aligned} \mathcal{L}'_N^{(1)} = \bar{N} & \left( i\not{\partial} - M_N - i \frac{g_A}{f} M_N \tau^a \pi^a \gamma_5 + \frac{g_A^2}{2f^2} M_N \pi^2 \right. \\ & \left. - \frac{(g_A - 1)^2}{4f^2} \tau^a \varepsilon^{abc} \pi^b \not{\partial} \pi^c \right) N + \mathcal{O}(\pi^3). \end{aligned} \quad (14)$$

The major difference between the two forms is that the pseudovector  $\pi NN$  coupling is transformed into a pseudoscalar one, while the Weinberg–Tomozawa  $\pi\pi NN$  term, which resembles a  $\rho$ -meson exchange, gets replaced by an isoscalar term akin to the remains of an integrated-out  $\sigma$ -meson in the linear  $\sigma$  model. The isovector  $\pi\pi NN$  term, which is now proportional to  $(g_A - 1)^2$ , does not give any contribution to Compton amplitude at one-loop level.

Also, in the NLO loops, the photon couples only minimally, i.e., to the electric charge of the pion and nucleon. Now that the pion couples to the nucleon via pseudoscalar coupling, there is no Kroll–Ruderman ( $\gamma\pi NN$ ) term arising, and hence the number of one-loop graphs is reduced. The resulting expressions for amplitudes become simpler.

As a result, the loop graphs shown in Fig. 2 with couplings from the Lagrangian Eq. (13) transform to the graphs shown in Fig. 3 with the couplings from Eq. (14). We have also checked explicitly that the two sets of one-loop diagrams give identical expressions for the Compton amplitude.

Although the main purpose of the above field redefinition is to simplify the calculation, it does give more insight about the chiral dynamics. First of all, it explains how Metz and Drechsel [64], calculating polarizabilities in the linear  $\sigma$  model with a heavy  $\sigma$ -meson, obtain to one loop exactly the same result as B $\chi$ Pt at  $\mathcal{O}(p^3)$  [36]. Secondly, observing that graphs

(12) and (13) vanish in the forward kinematics, we can see that chiral symmetry plays less of a role in the forward Compton scattering at order  $p^3$ .

Going to  $\mathcal{O}(p^4/\Delta)$  we encounter the graphs with one  $\Delta$ -isobar propagator shown in Fig. 4. The nucleon-field redefinition does not affect these contributions at this order.

Note that the graphs where photons couple minimally to  $\Delta$  contain more than one  $\Delta$  propagator and therefore should be suppressed by extra powers of  $p/\Delta$ . However, their lower-order contributions are important for electromagnetic gauge invariance and therefore for the renormalization program. In particular, the lower-order contributions of chiral loops should not affect the result of the low-energy theorem (LET) [67], and this condition is automatically satisfied for a subclass of graphs which obeys gauge invariance. The loop graphs in Fig. 4 form such a subclass for the case of neutral  $\Delta$ . In reality the  $\Delta$  comes in four charge states (isospin 3/2), and hence a gauge invariant set will in addition have the higher-order graphs where photon couples minimally to the  $\Delta$ . To make the subclass of loop graphs in Fig. 4 gauge invariant without the higher-order graphs, we used the following procedure:

- The one-particle-irreducible (1PI) graphs, Fig. 4(15–18) are computed with the correct isospin factors, i.e., summing over all charge states of the  $\Delta$ . The isospin factors for the one-particle reducible (1PR) graphs (19–22) are chosen such that their ratio to the isospin factors of 1PI graphs is the same as in the neutral  $\Delta$  case.

This procedure automatically ensures exact gauge invariance and thus effectively includes the lower-order contributions of the one-loop graphs with minimal coupling of photons to the  $\Delta$ . In case when the latter graphs are included explicitly, the isospin factors of 1PR graphs can be restored to actual values. This, however, will not affect the result at the order considered here.

The graphs in Fig. 3 and in Fig. 4 were eventually computed by us with the help of the symbolic manipulation tool FORM [65] and the LoopTools library [66] using dimensional regularization.

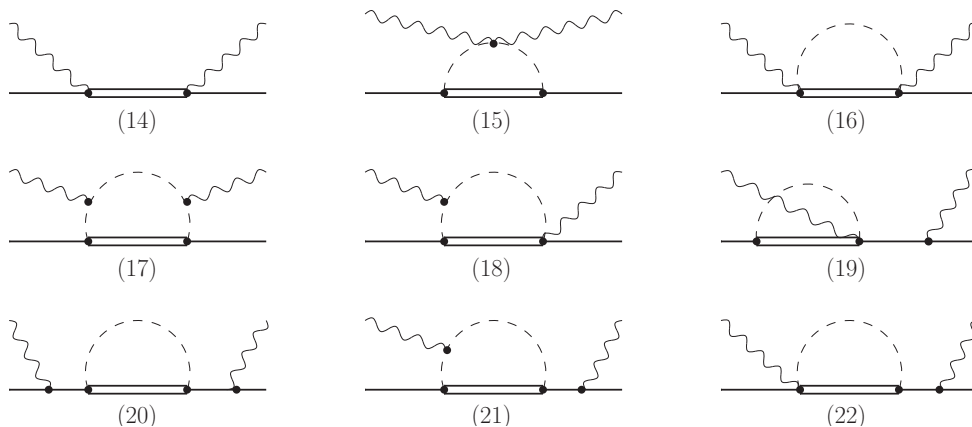


FIG. 4: The NNLO graphs evaluated in this work. Double lines denote the propagator of the  $\Delta$ . Graphs obtained from these by crossing and time reversal are not shown, but are evaluated too.

## B. Renormalization

In accordance with the LET [67], the loop contributions shown in Fig. 3 and in Fig. 4 may contribute to the renormalization of nucleon mass, field, charge, and anomalous magnetic moment. We have adopted the on-mass-shell renormalization scheme, not the extended on-mass-shell renormalization (EOMS) [40]. The difference is that in EOMS the above-listed quantities are taken to be at their chiral limit value while here we simply take the values at the actual pion mass, see, e.g., Table II.

Let us discuss first the contributions to nucleon self-energy and  $\gamma NN$  vertex corresponding to the nucleon loops (5–7) in Fig. 3. The corresponding amputated diagrams give contributions to nucleon self-energy (5) and to  $\gamma NN$  vertex (6), (7). More specifically, the contributions to the self-energy and the  $\gamma NN$  vertex can be written in the following form:

$$i\Sigma(\not{p}) = i\Sigma(M_N) + i(\not{p} - M_N)\Sigma'(M_N) + S(\not{p} - M_N), \quad (15)$$

$$i\Gamma^\mu(p, p_s) = i\gamma^\mu F_1(p_s^2) - i\gamma^{\mu\nu} q_\nu F_2(p_s^2) + i\not{q}p^\mu F_3(p_s^2) + i(\not{p}_s - M_N)\gamma^\mu F_4(p_s^2), \quad (16)$$

where  $p$  is the initial nucleon momentum,  $q$  is the initial photon momentum, and  $p_s = p + q$ . The function  $S$  is finite and its expansion in powers of  $\not{p} - M_N$  starts from a quadratic term. Of all the functions  $F_1 \dots F_4$  that contribute to the  $\gamma NN$  vertex only  $F_1$  is divergent. It contributes to the renormalization of charge. Function  $F_2$  contributes to a renormalization of the nucleon's anomalous magnetic moment. In this case the renormalization is finite [48].

After the renormalization, the self-energy and the  $\gamma NN$  vertex can be written in the following form:

$$i\Sigma_R(\not{p}) = i\Sigma(\not{p}) - i\Sigma(M_N) - i(\not{p} - M_N)\Sigma'(M_N) = S(\not{p} - M_N) \quad (17)$$

$$i\Gamma_R^\mu(p, p_s) = i\gamma^\mu \bar{F}_1(p_s^2) - i\gamma^{\mu\nu} q_\nu \bar{F}_2(p_s^2) + i\not{q}p^\mu F_3(p_s^2) + i(\not{p}_s - M_N)\gamma^\mu F_4(p_s^2), \quad (18)$$

where  $\bar{F}_{1,2}(p_s^2) = F_{1,2}(p_s^2) - F_{1,2}(M_N^2)$  are subtracted functions. Note that functions  $F_3(p_s^2)$  and  $F_4(p_s^2)$  do not get subtracted; indeed, the Lorentz structures that correspond to these functions are purely off-shell — they give zero when both nucleons are on-shell (i.e., when both  $p$  and  $p_s$  are on-shell momenta), so they do not contribute to the renormalization of charge or magnetic moment. However, both these functions play an important role in making the complete Compton scattering amplitude gauge invariant. Note also the fact that after the renormalization of nucleon mass, wave function, charge, and anomalous magnetic moment is performed, the remaining expressions for the nucleon loops (5–7) become finite.

Now we come to the loops with  $\Delta$ , Fig. 4. The corresponding amputated loops also give contributions to nucleon self-energy and to  $\gamma NN$  vertex, and the corresponding expressions can be written in a full analogy to the case of nucleon loops. The loop (19) in Fig. 4 also gives a contribution to  $\gamma NN$ , however, this contribution is fully off-shell and momentum-independent:

$$i\Gamma^\mu(p, p_s) = i\not{q}p^\mu A + i(\not{p}_s - M_N)\gamma^\mu B, \quad (19)$$

where  $A$  and  $B$  are constants. Nevertheless, it is important to take this contribution into account in order to preserve the electromagnetic gauge invariance. The renormalization of

nucleon self-energy and  $\gamma NN$  vertex proceeds for these loops in complete analogy to the purely nucleon loops.

In the case of  $\Delta$  loops, however, we obtain in addition some higher-order divergences, i.e., ultraviolet divergences of  $\mathcal{O}(p^4)$ . They are to be renormalized by a corresponding  $\mathcal{O}(p^4)$  contact term. At this stage it is customary to use the  $\overline{MS}$  subtraction of the higher-order divergences, see e.g., Ref. [68]. We have implemented the  $\overline{MS}$  scheme for the higher-order divergences by putting the dimreg factor equal to zero (see Appendix A for more detail).

### C. Consistency with forward-scattering sum rules

The dispersion relations enjoy a special role in nucleon Compton scattering, see Ref. [1] for a review. First of all, practically all up-to-date empirical values of nucleon polarizabilities are extracted from data with the use of a model based on dispersion relations [15, 16]. Secondly, in the forward kinematics, the Compton amplitude can be related to an integral over energy of the photoabsorption cross section, which in combination with the low-energy expansion yields a number of model-independent sum rules. A famous example is the Baldin sum rule:

$$\alpha + \beta = \frac{1}{2\pi^2} \int_0^\infty d\nu \frac{\sigma_{\text{tot}}(\nu)}{\nu^2 - i0}, \quad (20)$$

where the sum of polarizabilities is related to an integral of the total photoabsorption cross section  $\sigma_{\text{tot}}$  over the photon lab-frame energy  $\nu$ .

In general, the forward Compton-scattering amplitude can be decomposed into two scalar functions of a single variable in the following way:

$$T_{fi}(\nu) = \vec{\epsilon}'^* \cdot \vec{\epsilon} f(\nu) + i\vec{\sigma} \cdot (\vec{\epsilon}'^* \times \vec{\epsilon}) \nu g(\nu), \quad (21)$$

where  $\vec{\epsilon}'$ ,  $\vec{\epsilon}$  are the polarization vectors of the initial and final photons, respectively, and  $\vec{\sigma}$  are the Pauli spin matrices. The functions  $f$  and  $g$  are even functions of  $\nu$ . Using analyticity and the optical theorem, one can write down the following sum rules:

$$f(\nu) = f(0) + \frac{\nu^2}{2\pi^2} \int_0^\infty d\nu' \frac{\sigma_{\text{tot}}(\nu')}{\nu'^2 - \nu^2 - i0}, \quad (22a)$$

$$g(\nu) = \frac{1}{4\pi^2} \int_0^\infty d\nu' \nu' \frac{\sigma_{1/2}(\nu') - \sigma_{3/2}(\nu')}{\nu'^2 - \nu^2 - i0}, \quad (22b)$$

where  $f(0) = -e^2/M_N$  is the Thomson amplitude and  $\sigma$  is the doubly polarized photoabsorption cross section, with the index indicating the helicity of the initial photon–nucleon state;  $\sigma_{\text{tot}} = \frac{1}{2}(\sigma_{1/2} + \sigma_{3/2})$ .

These sum rules should also hold for the individual contributions of the loop graphs in Fig. 3. In this case the photoabsorption process is given by the Born graphs of single-pion

photoproduction, for which analytic expressions exist [48, 69]:

$$\begin{aligned}
\sigma_{1/2}^{(\pi^0 p)} + \sigma_{3/2}^{(\pi^0 p)} &= \frac{\pi C}{M_N \nu^3} \left\{ [\nu^2 - \mu^2 x_N s] \ln \frac{x_N + \lambda}{x_N - \lambda} + 2\lambda [\nu^2 (x_N - 2) + s\mu^2] \right\}, \\
\sigma_{1/2}^{(\pi^+ n)} + \sigma_{3/2}^{(\pi^+ n)} &= \frac{2\pi C}{M_N \nu^3} \left\{ -x_\pi s \mu^2 \ln \frac{x_\pi + \lambda}{x_\pi - \lambda} + 2\lambda (x_N \nu^2 + s\mu^2) \right\}, \\
\sigma_{1/2}^{(\pi^0 p)} - \sigma_{3/2}^{(\pi^0 p)} &= \frac{\pi C}{\nu^2} \left\{ -\left(2x_N \frac{s}{M_N^2} + 1 - \frac{\nu}{M_N}\right) \ln \frac{x_N + \lambda}{x_N - \lambda} \right. \\
&\quad \left. + 2\lambda \left[ \frac{\nu}{M_N} (x_N - 2) + \frac{s}{M_N^2} (x_N + 2) \right] \right\}, \\
\sigma_{1/2}^{(\pi^+ n)} - \sigma_{3/2}^{(\pi^+ n)} &= \frac{2\pi C}{\nu^2} \left\{ \mu^2 \ln \frac{x_\pi + \lambda}{x_\pi - \lambda} - 2\lambda \left( \frac{s}{M_N^2} x_\pi - \frac{\nu}{M_N} x_N \right) \right\},
\end{aligned} \tag{23}$$

where  $C = [eg_A M_N / (4\pi f_\pi)]^2$ ,  $\mu = m_\pi / M_N$ ,  $s = M_N^2 + 2M_N \nu$ , and

$$\begin{aligned}
x_N &= (s + M_N^2 - m_\pi^2) / 2s, \\
x_\pi &= (s - M_N^2 + m_\pi^2) / 2s, \\
\lambda &= (1/2s) \sqrt{s - (M_N + m_\pi)^2} \sqrt{s - (M_N - m_\pi)^2},
\end{aligned} \tag{24}$$

are the fractions of nucleon and pion energy ( $x$ ) and momentum ( $\lambda$ ) in the center-of-mass frame.

We have verified indeed that the (renormalized)  $p^3$  loop contributions in Fig. 3 fulfill the sum rules in Eq. (22) exactly for any positive  $\nu$ .

It is interesting to note that the leading-order pion photoproduction amplitude, which enters on the right-hand side of Eq. (22), is independent of whether one uses pseudovector or pseudoscalar  $\pi NN$  coupling [69]. It essentially means that chiral symmetry of the effective Lagrangian plays no role at this order. The latter statement can, by means of the sum rule, be extended to the forward Compton amplitude at  $\mathcal{O}(p^3)$ . On the other hand, the graphs (12) and (13) in Fig. 3, being the only ones beyond the pseudoscalar theory, take the sole role of chiral symmetry. In the forward kinematics these graphs indeed vanish but play an important role in the backward angles. Without them the values of  $\alpha$  and  $\beta$  would be entirely different. The value of  $\alpha + \beta$  would of course be the same, but  $\alpha - \beta$  would (approximately) flip sign. Furthermore, in the chiral limit, the value of  $\alpha - \beta$  would diverge as  $1/m_\pi^2$  (instead of  $1/m_\pi$  as it should). We thus arrive at the conclusion that chiral symmetry of the effective Lagrangian plays a more prominent role in backward Compton scattering.

#### D. Error due to $\mathcal{O}(p^4)$ effects

In the previous publication [54] we simply adopted the error estimate from Ref. [43]. However, in this work we compute to one order higher than in Ref. [43] and hence the error analysis needs to be revised accordingly.

An error of an effective-field theory calculation is an estimate of higher-order effects assuming their natural size. The higher-order effects not included in our calculation begin at  $\mathcal{O}(p^4)$ , i.e., the order at which the polarizability LECs,  $\delta\alpha$  and  $\delta\beta$ , arise. The naturalness assumption requires these constants to be of order of unity in the units of the chiral symmetry

breaking scale of a GeV. To be more specific we assume the absolute value of these constants (in the  $\overline{MS}$  scheme) is limited by

$$\alpha_{(err.)} = \beta_{(err.)} = (e^2/4\pi)/M_N^3 \approx 0.7 \times 10^{-4} \text{ fm}^3, \quad (25)$$

This number gives a natural estimate of the error on polarizability values we have obtained at NNLO. It is not difficult to find how this error propagates to observables, once the effect of the LECs on those observables is known. For example, for the unpolarized differential cross section, the error is given by [cf. Eq. (32)]:

$$\frac{d\sigma^{(err.)}}{d\Omega} = 8 (e^2/4\pi) \Phi \nu \nu' [(1+z)^2 \alpha_{(err.)}^2 + (2z)^2 \beta_{(err.)}^2]^{1/2} \quad (26)$$

where  $z = \cos \theta_{\text{lab}}$ ,  $\nu$  ( $\nu'$ ) the laboratory energy of the incident (scattered) photon, and

$$\Phi = \begin{cases} \frac{1}{4s} & \text{(center-of-mass frame),} \\ \frac{1}{4M_N^2} \left(\frac{\nu'}{\nu}\right)^2 & \text{(lab frame).} \end{cases} \quad (27)$$

Let us emphasize that we do not include the errors due to the uncertainty in the values of parameters in Table II or due to the  $\mathcal{O}(p^5/\Delta^2)$  effects which stem from graphs with two  $\Delta$  propagators. Our errors are thus underestimated, however, they can directly serve as an indicator of sensitivity to the polarizability LECs at  $\mathcal{O}(p^4)$ .

#### IV. PROTON POLARIZABILITIES

The chiral-loop contribution to scalar polarizabilities of the proton which arise from the NNLO calculation of the Compton amplitude is given in the Appendix A. In addition, we have the tree-level  $\Delta(1232)$  contribution from graphs (14) in Fig. 4 and its crossed, given by [43]:

$$\alpha(\Delta\text{-excit.}) = -\frac{2e^2 g_E^2}{4\pi(M_N + M_\Delta)^3} \simeq -0.1, \quad (28)$$

$$\beta(\Delta\text{-excit.}) = \frac{2e^2 g_M^2}{4\pi(M_N + M_\Delta)^2 \Delta} \simeq 7.1. \quad (29)$$

Here and in what follows the numerical values are given in the units of  $10^{-4} \text{ fm}^3$ .

The numerical composition of the full result thus looks as follows:

$$\alpha = \underbrace{6.8}_{\mathcal{O}(p^3)} + \underbrace{(-0.1)}_{\mathcal{O}(p^4/\Delta)} + 4.1 = 10.8, \quad (30)$$

$$\beta = \underbrace{-1.8}_{\mathcal{O}(p^3)} + \underbrace{7.1 - 1.3}_{\mathcal{O}(p^4/\Delta)} = 4.0. \quad (31)$$

As explained earlier, a natural estimate of  $\mathcal{O}(p^4)$  contributions yields an uncertainty of at least  $\pm 0.7$  on these values. In Fig. 5 this result, shown by the red blob, is compared with the empirical information, and with the  $\Delta$ -less  $\mathcal{O}(p^4)$  HB $\chi$ PT result of Beane et al. [42].

We can clearly see a few-sigma discrepancy of our result with the TAPS-MAMI determination of polarizabilities [9]. On the other hand, as shown in the next section, our result

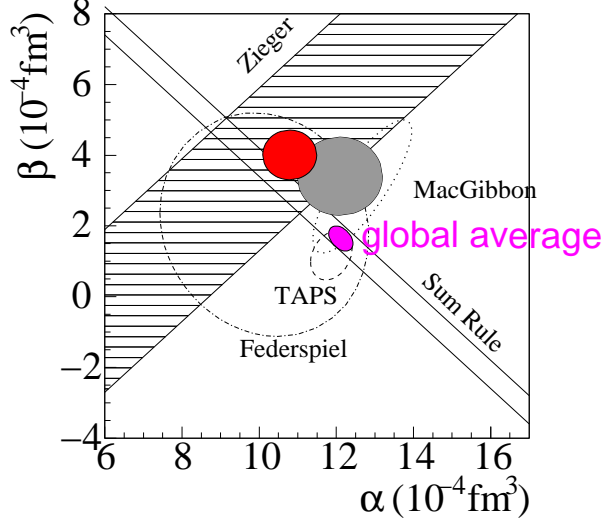


FIG. 5: (Color online) The scalar polarizabilities of the proton. Our result is shown by the red blob. The  $\Delta$ -less HB $\chi$ PT result [42] is shown by the grey blob. Experimental results are from Federspiel et al. [5], Zieger et al. [6], MacGibbon et al. [8], and TAPS [9]. “Sum Rule” indicates the Baldin sum rule constraint on  $\alpha + \beta$  [70]. “Global average” represents the PDG summary [37].

agrees with TAPS data for the Compton differential cross sections. Of course we compare with the data at the lower energy end (below the pion threshold) where polarizabilities play the prominent role. The extraction of the polarizabilities in Ref. [9] has also been influenced by data above the  $\Delta$ -resonance region to which we cannot compare. Clearly an extraction of scalar polarizabilities based on the data of 400 MeV and higher could be affected by uncontrolled model dependencies and needs to be avoided. Excluding the higher-energy data from the TAPS analysis could help to resolve the apparent discrepancy between theory and experiment in Fig. 5.

In Fig. 6 we show the pion mass dependence of proton polarizabilities in both B $\chi$ PT and HB $\chi$ PT. The difference between the two for the magnetic polarizability (lower panel) at  $\mathcal{O}(p^3)$  is stunning (compare the blue dashed and violet dotted curves). The region of applicability of the HB expansion is apparently limited here to essentially the chiral limit,  $m_\pi \rightarrow 0$ . For any finite pion mass, the B $\chi$ PT and HB $\chi$ PT results come out to be of a similar magnitude but of the opposite sign. A similar picture is observed for the  $\pi\Delta$  loops arising at  $\mathcal{O}(p^4/\Delta)$ . In fact, we have checked that in the limit of vanishing  $\Delta$ -nucleon mass splitting ( $\Delta \rightarrow 0$ ), the considered  $\pi N$  and  $\pi\Delta$  loops give (up to the spin-isospin factors) the same result.

The total effect of the Delta here is the difference between the  $\mathcal{O}(p^3)$  and the  $\mathcal{O}(p^4/\Delta)$  curves in B $\chi$ PT and the difference between the  $\mathcal{O}(p^3)$  and the  $\mathcal{O}(\epsilon^3)$  curves in HB $\chi$ PT. Note that here the  $\mathcal{O}(\epsilon^3)$  contribution in HB $\chi$ PT with  $\Delta(1232)$  precisely corresponds to  $\mathcal{O}(p^4/\Delta)$  of B $\chi$ PT, thus we do not include the  $\mathcal{O}(p^4)$  LECs in neither of the calculations. The actual  $\mathcal{O}(\epsilon^3)$  calculations [44] are supplemented with the  $\mathcal{O}(p^4)$  LECs, whose main role is then to cancel the large contribution of the  $\Delta$ -isobar.

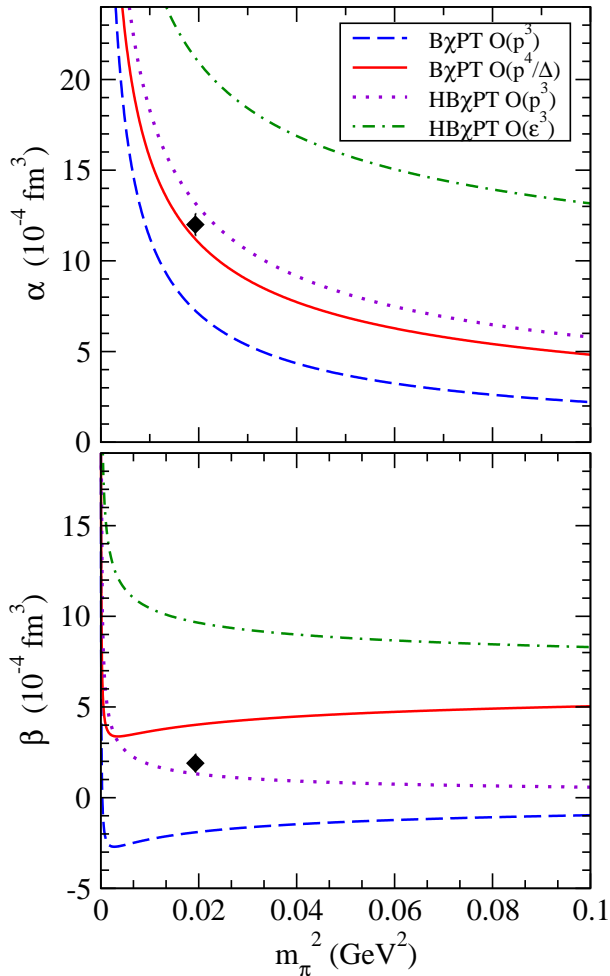


FIG. 6: (Color online) The pion-mass dependence of proton polarizabilities. Data points at the physical pion mass represent the PDG values. The legend for the curves is in the upper panel.

## V. RESULTS FOR CROSS SECTIONS

In this section we present the results for the differential cross sections of proton Compton scattering.

### A. Unpolarized

In Fig. 7, we consider the unpolarized differential cross section of the  $\gamma p \rightarrow \gamma p$  process as a function of the scattering angle in center-of-mass system, at fixed incident photon energy. In Fig. 8, we study the same cross section, but as a function of the energy for fixed scattering angle in the lab frame. Our complete NNLO result is shown by red solid curves with band indicating the theory error estimate given in Eq. (26). The agreement between the theory and the experiment is quite remarkable here, especially given the fact that the theory result here is a prediction in the sense that has no free parameters. Despite this good agreement, as already noted above, there is a few-sigma discrepancy in the polarizability values between this theoretical prediction and the most precise empirical extraction [9]. This is apparently

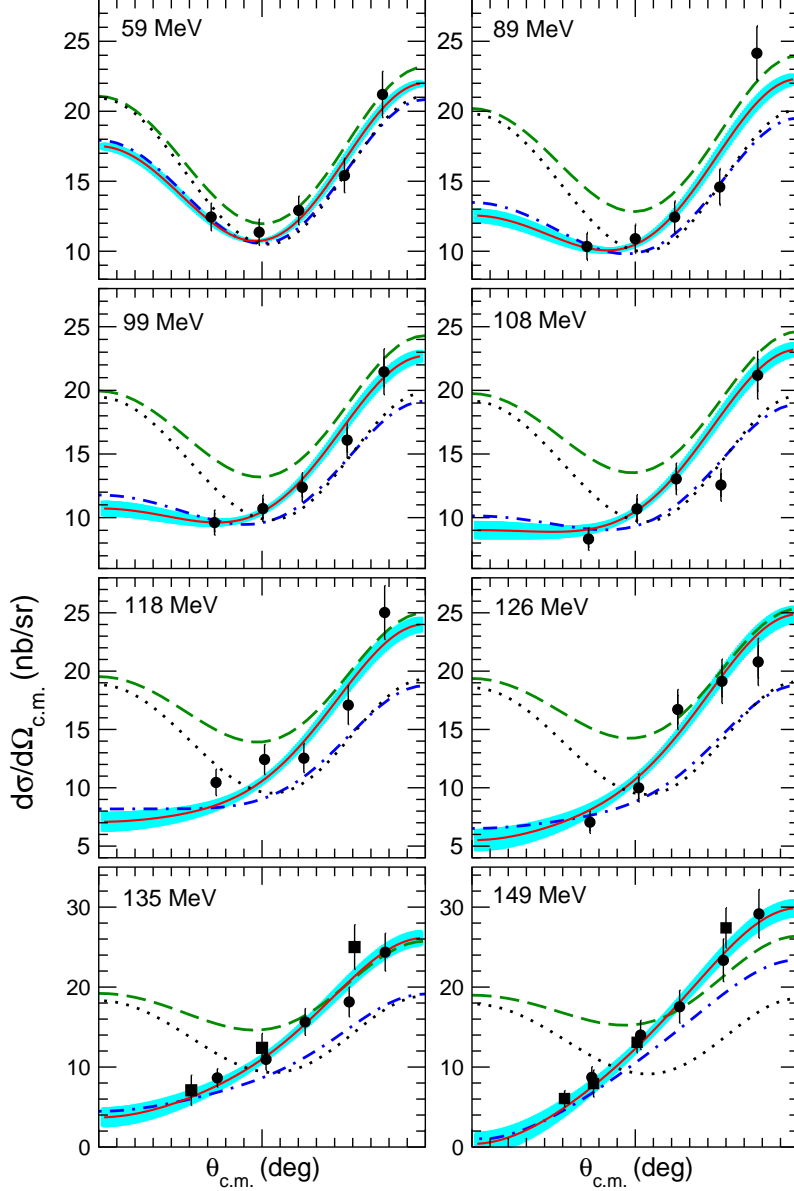


FIG. 7: (Color online) Angular dependence of the  $\gamma p \rightarrow \gamma p$  differential cross section in the center-of-mass system for a fixed photon-beam energies as specified for each panel. Data points are from SAL [7] — filled squares, and MAMI [9] — filled circles. The curves are: Klein–Nishina — dotted, Born graphs and WZW-anomaly — green dashed, adding the  $p^3$   $\pi N$  loop contributions of B $\chi$ PT — blue dash-dotted. The result of adding the  $\Delta$  contributions, i.e., the complete NNLO result, is shown by the red solid line with band.

because the data at higher energies used additionally in the empirical extraction play an important role in the determination of  $\beta$ .

It is always interesting to study the convergence of the chiral expansion. In these figures the leading-order,  $\mathcal{O}(p^2)$ , result is shown by dotted curve, which is nothing else than the Klein–Nishina cross section (i.e, Compton scattering off a classical pointlike particle with the charge and mass of the proton). The NLO,  $\mathcal{O}(p^3)$ , result is given by the blue dash-dotted curve. One can see that the size of the effects varies strongly with the scattering angle.

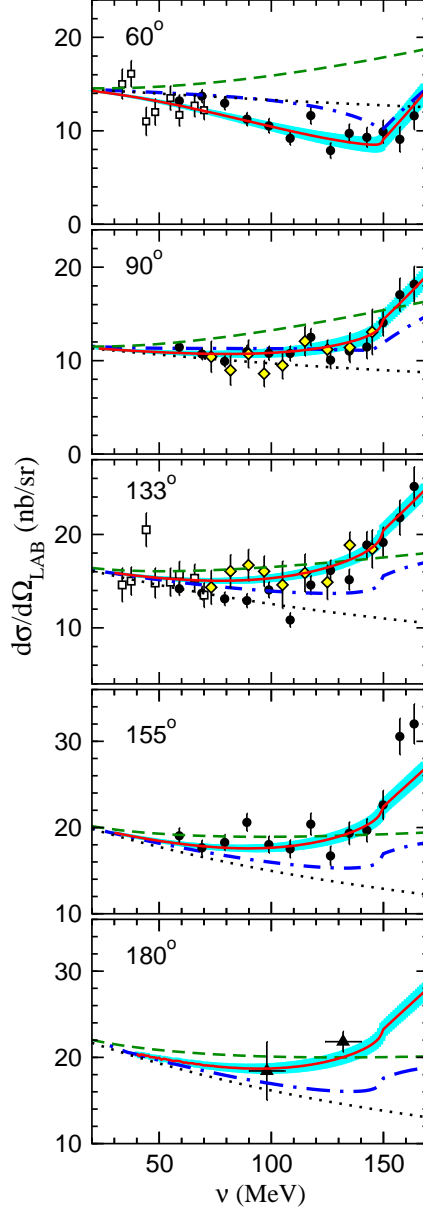


FIG. 8: (Color online) Energy dependence of the  $\gamma p \rightarrow \gamma p$  differential cross section in the lab frame for fixed values of the scattering angle. Data points are from: Illinois [5] — open squares, MAMI [6] — filled triangles, SAL [8] — open diamonds, and MAMI [9] — filled circles. The legend for the curves is the same as in Fig. 7.

At energies below the pion-production threshold, the NLO effects are tiny at backward angles but play a crucial role at forward angles. The situation is quite the opposite for the NNLO  $\Delta$ -isobar contributions. Nevertheless, the convergence of this expansion seems to be satisfactory and in any case is much better than it would be in analogous HB $\chi$ PT calculations.

For completeness the result for the Born contribution, given by the Powell cross section together with the WZW anomaly contribution (graphs in Fig. 1), is shown here by the green dashed curves. Any deviation from these curves at low energies is attributed to polarizability

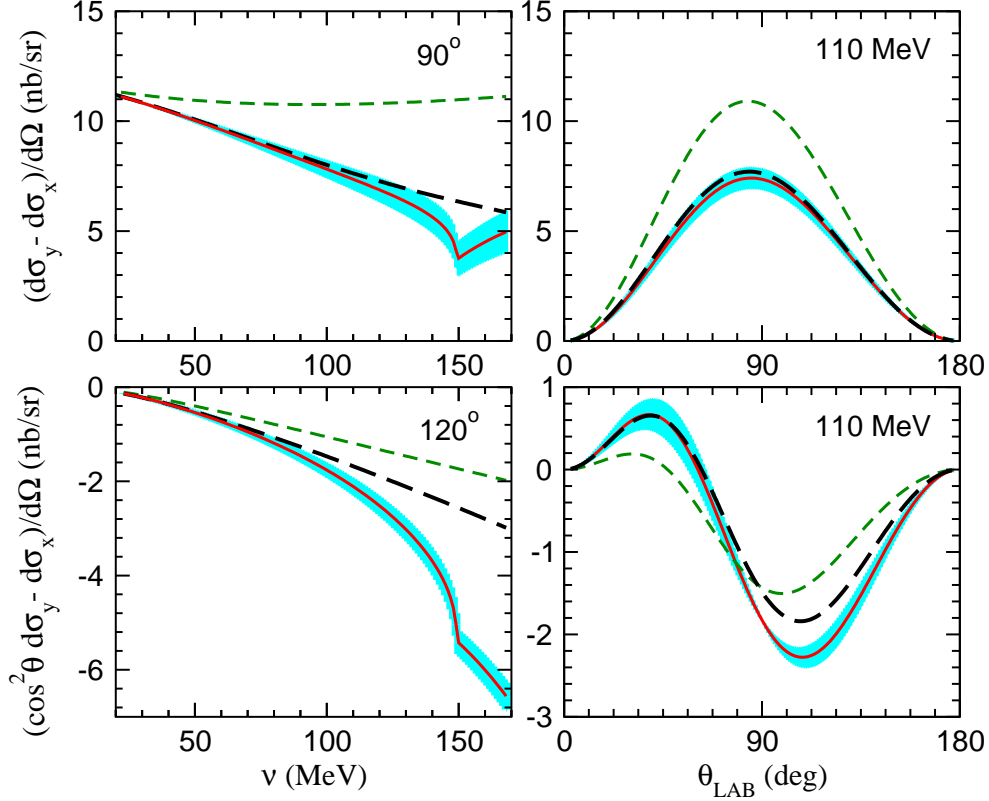


FIG. 9: (Color online) Linearly polarized differential cross sections as defined in the text for fixed values of the scattering angle (left panel) or fixed energy (right panel). The green dashed curves — Born graphs and WZW-anomaly; black long-dashed — in upper panels result of adding  $\alpha = 10.8$ , in lower panels result of adding  $\beta = 4$ , both using LEX. The NNLO result is shown by the red solid line with band.

effects. More specifically,

$$\frac{d\sigma}{d\Omega} - \frac{d\sigma^{(\text{Born})}}{d\Omega} = -8(e^2/4\pi) \Phi \nu \nu' \left[ \frac{1}{2}(\alpha + \beta)(1 + z)^2 - \frac{1}{2}(\alpha - \beta)(1 - z)^2 \right] + \mathcal{O}(\nu^3), \quad (32)$$

where  $\Phi$  is defined in Eq. (27) and  $z$  is the cosine of the lab-frame scattering angle.

The difference between the dashed (Born) curves and the dotted (Klein–Nishina) curves arises mainly due to proton’s anomalous magnetic moment. The difference is substantial but at backward angles can be seen to cancel almost entirely against the chiral loop contribution at  $\mathcal{O}(p^3)$ , to obtain the blue curves. Thus, at  $\mathcal{O}(p^3)$ , there is an intricate cancellation between the anomalous magnetic moment and the chiral loop effects. It would be interesting to see if this cancellation persists at higher orders.

## B. Polarized

In Fig. 9 we show the results for Compton-scattering differential cross sections obtained with linearly polarized beam. The subscript  $x$  ( $y$ ) indicates that the beam polarization is parallel (perpendicular) to the scattering plane,  $\theta$  is the scattering angle in the lab frame and  $d\Omega = -2\pi \sin \theta d\theta$ . The two particular combinations of polarized cross sections, seen

in the upper and the lower panels, are chosen such that each of them is sensitive to only one of the polarizabilities. They are therefore selected for the forthcoming measurement of proton polarizabilities at the HIGS facility [71]. The HIGS measurements are planned to be taken at 110 MeV photon lab energy, where a low-energy expansion (LEX) is assumed to hold. Indeed a study of the unpolarized differential cross section indicates that LEX can be trusted to energies of about 100 MeV [8]. Here we make a similar study for the polarized cross sections.

The LEX states that at the second order the deviation of the polarized cross sections from the corresponding Born result (dashed lines in the figure) is simply given in terms of the polarizabilities:

$$\frac{d\sigma_x}{d\Omega} - \frac{d\sigma_x^{(\text{Born})}}{d\Omega} = -8(e^2/4\pi) \Phi \nu \nu' (\alpha \cos \theta + \beta) \cos \theta + \mathcal{O}(\nu^3) \quad (33a)$$

$$\frac{d\sigma_y}{d\Omega} - \frac{d\sigma_y^{(\text{Born})}}{d\Omega} = -8(e^2/4\pi) \Phi \nu \nu' (\alpha + \beta \cos \theta) + \mathcal{O}(\nu^3), \quad (33b)$$

where  $\Phi$  is defined in Eq. (27). A derivation of these expressions is given in Appendix B.

From Eq. (33) one can indeed see that, at this order in LEX, the difference of the polarized cross sections,  $d\sigma_y/d\Omega - d\sigma_x/d\Omega$ , is proportional to  $\alpha$ , while the combination  $\cos^2 \theta d\sigma_y/d\Omega - d\sigma_x/d\Omega$  is proportional to  $\beta$ . One should realize, though, that this is only an approximate result which breaks down at sufficiently high energies. The Fig. 9 attempts to address this issue in a quantitative way by comparing the second-order LEX (long-dashed curves) with the result of NNLO B $\chi$ PT (red solid curves with the error band). The LEX and B $\chi$ PT results have exactly the same values for the polarizabilities  $\alpha$  and  $\beta$ , but the validity of B $\chi$ PT extends over the whole considered energy range.

We conclude that a determination at 110 MeV based on a second-order LEX can be reliable for  $\alpha$ , see the upper panels. The situation is not as fortunate for the observable aimed at the determination of  $\beta$ , see the lower panels. The LEX result begins to fail here at lower energies, at least in the backward angles where Compton experiments are usually simpler.

## VI. CONCLUSION

We have completed a next-to-next-to-leading order (NNLO) calculation of low-energy Compton scattering on the proton within the  $\chi$ PT framework. More specifically, we have computed all the effects of order  $p^2$ ,  $p^3$ , and  $p^4/\Delta$ , with  $\Delta$  being the excitation energy of the  $\Delta(1232)$  resonance. These are all *predictive* powers in the sense that no unknown low-energy constants (LECs) enter until at least one order higher [i.e.,  $\mathcal{O}(p^4)$ ]. This fact together with the availability of precise data for Compton scattering has given us a unique opportunity to put  $\chi$ PT to a test.

We have found that, assuming a natural size of the  $\mathcal{O}(p^4)$  LECs, the theoretical uncertainty of the NNLO calculation is comparable with the uncertainty of present empirical information about the cross sections of proton Compton scattering and the corresponding values for isoscalar polarizabilities of the proton. Within these uncertainties the NNLO result agrees with the cross sections data below the pion threshold but shows a three-sigma discrepancy in the value for the magnetic polarizability. We note that the state-of-the-art empirical value for the polarizabilities was extracted by using not just the low-energy data

but also data above the  $\Delta$ -resonance region. The planned experiments at HIGS could be very helpful in sorting out this issue, since they plan to use precision low-energy data only. In this case, however, the reliance on the strict second-order low-energy expansion might be a problem, as our calculation has shown. The  $\chi$ PT framework itself could provide a more reliable energy interpolation needed for the extraction of polarizabilities.

In this work we have insisted on the fact that *chiral power counting* should be done for *graphs*, not *contributions*. It does not put any constraint on how many powers of pion mass or energy may appear in the result. It puts the constraint on the leading power only. The heavy-baryon expansion is therefore not mandatory for correct power-counting. What is important is that no powers lower than given by power-counting are present in the result. The manifestly covariant baryon  $\chi$ PT (B $\chi$ PT) conforms to this requirement, because even if the lower-order terms appear in calculation of a given graph, they are shown to contribute only to a renormalization of the LECs. In our example, the low-energy theorem and chiral symmetry ensured that all such troublesome terms contributed only to the renormalization of nucleon mass, charge, and the anomalous magnetic moment.

## Acknowledgments

We would like to thank Daniel Phillips and Marc Vanderhaeghen for a number of illuminating discussions, and Martin Schumacher for a helpful communication. V. L. is grateful to the Institut für Kernphysik at Johannes Gutenberg Universität Mainz for kind hospitality.

## APPENDIX A: CHIRAL LOOP CONTRIBUTIONS TO POLARIZABILITIES

Hereby we give the expressions for the loop contributions of  $\mathcal{O}(p^3)$  and  $\mathcal{O}(p^4/\Delta)$  to isoscalar proton polarizabilities  $\alpha$  and  $\beta$ , as well as the corresponding heavy-baryon results.

### 1. Nucleon Loops

Our results for the loop contributions at  $\mathcal{O}(p^3)$  agree with [36]:

$$\alpha = \frac{e^2 g_A^2}{192\pi^3 M_N f^2} \left\{ -1 + \int_0^1 \frac{dx}{[D_N(x)]^3} \left[ 2x^4(-3x^3 + 8x^2 - 9x + 5) \right. \right. \quad (\text{A1})$$

$$\left. \left. + x^2(9x^4 - 26x^3 + 29x^2 - 18x + 7)\mu^2 - (9x^5 - 33x^4 + 45x^3 - 27x^2 + 7x - 1)\mu^4 \right] \right\},$$

$$\beta = \frac{e^2 g_A^2}{192\pi^3 M_N f^2} \quad (\text{A2})$$

$$\times \left\{ 1 - \int_0^1 \frac{dx}{[D_N(x)]^2} \left[ 2x^2(6x^3 - 13x^2 + 9x - 1) + (9x^4 - 24x^3 + 21x^2 - 6x + 1)\mu^2 \right] \right\},$$

where  $\mu = m_\pi/M_N$ , and  $D_N(x) = \mu^2(1-x) + x^2$ .

The corresponding heavy-baryon result is obtained from these expressions by expanding in  $\mu$  and keeping the leading term only:

$$\alpha^{(HB)} = \frac{10e^2 g_A^2}{768\pi^2 f^2 m_\pi}, \quad (\text{A3})$$

$$\beta^{(HB)} = \frac{e^2 g_A^2}{768\pi^2 f^2 m_\pi}. \quad (\text{A4})$$

## 2. Delta Loops

The  $\mathcal{O}(p^4/\Delta)$  loops of Fig. 4 give the following contribution to polarizabilities:

$$\begin{aligned} \alpha = & \frac{e^2 h_A^2 M_N}{3456\pi^3 M_\Delta^2 f^2} \left\{ \frac{25}{2} + 8\delta - 3 \int_0^1 \frac{dx x^2}{[D_\Delta(x)]^2} [(1-x)(35-104x+17x^2+112x^3-60x^4 \right. \\ & + (105-273x+72x^2+92x^3)\delta + (105-269x+88x^2+72x^3)\delta^2 + (35-100x+64x^2)\delta^3) \\ & \left. - x(35-69x-40x^2+72x^3+(35-100x+64x^2)\delta)\mu^2] \right. \\ & \left. - 6 \int_0^1 dx x(12+9x-34x^2+3(4-5x)\delta) [\Xi - \log D_\Delta(x)] \right\}, \quad (\text{A5}) \end{aligned}$$

$$\begin{aligned} \beta = & \frac{e^2 h_A^2 M_N}{3456\pi^3 M_\Delta^2 f^2} \left\{ \frac{65}{6} - 8\delta + \int_0^1 \frac{dx x^2}{D_\Delta(x)} (9-32x+24x^2)(1+x+\delta) \right. \\ & \left. + 6 \int_0^1 dx x(12+7x+10x^2+3(-4+5x)\delta) [\Xi - \log D_\Delta(x)] \right\}, \quad (\text{A6}) \end{aligned}$$

where  $\mu = m_\pi/M_N$ ,  $\delta = \Delta/M_N$ , and  $D_\Delta(x) = (1-x)[(1+\delta)^2 - x] + x\mu^2$ . Furthermore, in these expressions we have  $\Xi = 2/(4-d) - \gamma_E + \log(4\pi\Lambda/M_N)$  the divergence in  $d$  dimensions, with  $\Lambda$  the dimreg scale. Thus, the  $\Delta$  loops contain an ultraviolet divergence which is to be renormalized by  $\mathcal{O}(p^4)$  LECs. We choose to define the values for these LECs in the  $\overline{MS}$  scheme, and hence put  $\Xi = 0$ .

Expanding these results in small  $\mu$  and  $\delta$  to leading order, we reproduce the heavy-baryon result for the  $\pi\Delta$ -loop contributions [45]:

$$\alpha^{(HB)} = \frac{e^2 h_A^2}{864\pi^3 f^2 \Delta} \left( 9 + \log \frac{2\Delta}{m_\pi} \right), \quad (\text{A7})$$

$$\beta^{(HB)} = \frac{e^2 h_A^2}{864\pi^3 f^2 \Delta} \log \frac{2\Delta}{m_\pi}. \quad (\text{A8})$$

## APPENDIX B: LOW-ENERGY EXPANSION FOR CROSS SECTIONS

The differential cross section is given in terms of the Compton amplitude by

$$\frac{d\sigma}{dt} = \frac{1}{16\pi(s-M_N^2)^2} \sum_{\lambda'\sigma'} |T_{\lambda'\sigma',\lambda\sigma}|^2, \quad (\text{B1})$$

where  $\lambda$  and  $\sigma$  are the target and the photon's helicities. The sum is over the final helicities, the initial ones are fixed. To find the low-energy expansion (LEX) of this quantity at the second order in energy, we can ignore the *spin-dependent* contribution and write the Compton amplitude as follows:

$$T_{\lambda'\sigma',\lambda\sigma} = (-A_1(s,t) \mathcal{E}'_{\sigma'} \cdot \mathcal{E}_\sigma + A_2(s,t) q \cdot \mathcal{E}'_{\sigma'} q' \cdot \mathcal{E}_\sigma) 2M_N \delta_{\lambda'\lambda}, \quad (\text{B2})$$

where  $A_i$  are scalar amplitudes dependent on the Mandelstam variables only,  $q$  ( $q'$ ) is the initial (final) photon 4-momentum, and

$$\mathcal{E}^\mu = \varepsilon^\mu - \frac{P \cdot \varepsilon}{P \cdot q} q^\mu, \quad (\text{B3})$$

$$\mathcal{E}'^\mu = \varepsilon'^\mu - \frac{P \cdot \varepsilon'}{P \cdot q'} q'^\mu \quad (\text{B4})$$

with  $\varepsilon$  the vectors of photon polarization, and  $P = p + p'$  the sum of the nucleon external momenta. Since

$$\sum_\sigma \varepsilon_\sigma^\mu \varepsilon_\sigma^{*\nu} = -g^{\mu\nu}, \quad \varepsilon_\sigma \cdot \varepsilon_\sigma^* = -1, \quad (\text{B5})$$

we have

$$\sum_\sigma \mathcal{E}_\sigma^\mu \mathcal{E}_\sigma^{*\nu} = -g^{\mu\nu} + \frac{P^\mu q^\nu + P^\nu q^\mu}{P \cdot q} - \frac{P^2 q^\mu q^\nu}{(P \cdot q)^2} \quad (\text{B6})$$

with  $P \cdot q = \frac{1}{2}(s - M_N^2 - u + M_N^2) = M_N(\nu + \nu')$ . We therefore obtain

$$\begin{aligned} \sum_{\lambda'\sigma'} |T_{\lambda'\sigma',\lambda\sigma}|^2 &= (2M_N)^2 (-A_1 \mathcal{E}_{\sigma\mu} + A_2 q_\mu q' \cdot \mathcal{E}_\sigma) (-A_1 \mathcal{E}_{\sigma\nu}^* + A_2 q_\nu q' \cdot \mathcal{E}_\sigma^*) \\ &\times \left( -g^{\mu\nu} + \frac{P^\mu q'^\nu + P^\nu q'^\mu}{P \cdot q} - \frac{P^2 q'^\mu q'^\nu}{(P \cdot q')^2} \right). \end{aligned}$$

We next take the Born contribution out of  $A_1$ :

$$\tilde{A}_1 = A_1 + e^2/M_N \quad (\text{B7})$$

and use the LEX:

$$\tilde{A}_1 = 4\pi(\alpha + \beta z) \nu\nu' + \mathcal{O}(\nu^3), \quad (\text{B8})$$

$$\tilde{A}_2 = -4\pi\beta + \mathcal{O}(\nu), \quad (\text{B9})$$

where  $z$  is the cosine of the lab-frame scattering angle,  $\alpha$  and  $\beta$  are respectively the electric and the magnetic polarizability.

At the second order in  $\nu$  for the non-Born (NB) contribution we thus have

$$\begin{aligned} \sum_{\lambda'\sigma'} |T_{\lambda'\sigma',\lambda\sigma}^{(NB)}|^2 &= -8M_N(4\pi e^2) \nu\nu' \left[ \alpha + \beta z + (\hat{q}' \cdot \epsilon_\sigma)^2 \beta - \frac{4\nu\nu'}{(\nu + \nu')^2} (\hat{q}' \cdot \epsilon_\sigma)^2 (\alpha + \beta) \right] \\ &= -8M_N(4\pi e^2) \nu\nu' \left[ (1 - (\hat{q}' \cdot \epsilon_\sigma)^2) \alpha + \beta z \right] + \mathcal{O}(\nu^3), \end{aligned} \quad (\text{B10})$$

where  $\hat{q}' = (1, \sqrt{1 - z^2}, 0, z)$ . Substituting in Eq. (B1) and selecting the appropriate photon polarization we arrive at Eq. (33).

---

[1] D. Drechsel, B. Pasquini and M. Vanderhaeghen, Phys. Rept. **378**, 99 (2003).

- [2] M. Schumacher, *Prog. Part. Nucl. Phys.* **55**, 567 (2005).
- [3] D. R. Phillips, arXiv:0903.4439 [nucl-th].
- [4] J. Schmiedmayer, P. Riehs, J. A. Harvey and N. W. Hill, *Phys. Rev. Lett.* **66**, 1015 (1991).
- [5] F. J. Federspiel *et al.*, *Phys. Rev. Lett.* **67**, 1511 (1991).
- [6] A. Zieger, R. Van de Vyver, D. Christmann, A. De Graeve, C. Van den Abeele and B. Ziegler, *Phys. Lett. B* **278**, 34 (1992).
- [7] E. L. Hallin *et al.*, *Phys. Rev. C* **48**, 1497 (1993).
- [8] B. E. MacGibbon, G. Garino, M. A. Lucas, A.M. Nathan, G. Feldman and B. Dolbilkin, *Phys. Rev. C* **52**, 2097 (1995).
- [9] V. Olmos de Leon *et al.*, *Eur. Phys. J. A* **10**, 207 (2001).
- [10] A. M. Baldin, *Nucl. Phys.* **18**, 310 (1960).
- [11] B. R. Holstein, *Comments Nucl. Part. Phys.* **20**, 301 (1992).
- [12] A. C. Hearn and E. Leader, *Phys. Rev.* **126**, 789 (1962).
- [13] W. Pfeil, H. Rollnik and S. Stankowski, *Nucl. Phys. B* **73**, 166 (1974).
- [14] I. Guiasu, C. Pomponiu and E. E. Radescu, *Annals Phys.* **114**, 296 (1978).
- [15] A. I. L'vov, *Sov. J. Nucl. Phys.* **34**, 597 (1981) [*Yad. Fiz.* **34**, 1075 (1981)].
- [16] A. I. L'vov, V. A. Petrun'kin and M. Schumacher, *Phys. Rev. C* **55**, 359 (1997).
- [17] D. Drechsel, M. Gorchtein, B. Pasquini and M. Vanderhaeghen, *Phys. Rev. C* **61**, 015204 (1999).
- [18] B. Pasquini, D. Drechsel and M. Vanderhaeghen, *Phys. Rev. C* **76**, 015203 (2007).
- [19] V. Pascalutsa and O. Scholten, *Nucl. Phys. A* **591**, 658 (1995).
- [20] O. Scholten, A. Y. Korchin, V. Pascalutsa and D. Van Neck, *Phys. Lett. B* **384**, 13 (1996).
- [21] T. Feuster and U. Mosel, *Phys. Rev. C* **59**, 460 (1999).
- [22] S. Kondratyuk and O. Scholten, *Nucl. Phys. A* **677**, 396 (2000); *Phys. Rev. C* **64**, 024005 (2001).
- [23] S. Capstick and B. D. Keister, *Phys. Rev. D* **46**, 84 (1992) [Erratum-ibid. *D* **46**, 4104 (1992)].
- [24] M. Chemtob, *Nucl. Phys. A* **473**, 613 (1987).
- [25] N. N. Scoccola and W. Weise, *Phys. Lett. B* **232**, 287 (1989).
- [26] S. Scherer and P. J. Mulders, *Nucl. Phys. A* **549**, 521 (1992).
- [27] W. Broniowski and T. D. Cohen, *Phys. Rev. D* **47**, 299 (1993).
- [28] N. N. Scoccola and T. D. Cohen, *Nucl. Phys. A* **596**, 599 (1996).
- [29] F. X. Lee, L. Zhou, W. Wilcox and J. C. Christensen, *Phys. Rev. D* **73**, 034503 (2006); A. Alexandru and F. X. Lee, in *Proc. of Science (Lattice 2008)*, arXiv:0810.2833 [hep-lat].
- [30] W. Detmold, B. C. Tiburzi and A. Walker-Loud, *Phys. Rev. D* **73**, 114505 (2006); in *Proc. of Science (Lattice 2008)*, arXiv:0809.0721 [hep-lat].
- [31] W. Detmold, B. C. Tiburzi and A. Walker-Loud, arXiv:0904.1586 [hep-lat].
- [32] H. Pagels, *Phys. Rept.* **16**, 219 (1975).
- [33] S. Weinberg, *Physica A* **96**, 327 (1979).
- [34] J. Gasser and H. Leutwyler, *Annals Phys.* **158** (1984) 142.
- [35] J. Gasser, M. E. Sainio and A. Svarc, *Nucl. Phys. B* **307**, 779 (1988).
- [36] V. Bernard, N. Kaiser and U.-G. Meißner, *Phys. Rev. Lett.* **67**, 1515 (1991); *Nucl. Phys. B* **373**, 346 (1992).
- [37] W. M. Yao *et al.* [Particle Data Group], *J. Phys. G* **33**, 1 (2006).
- [38] E. Jenkins and A. V. Manohar, *Phys. Lett. B* **255**, 558 (1991).
- [39] J. Gegelia and G. Japaridze, *Phys. Rev. D* **60**, 114038 (1999); J. Gegelia, G. Japaridze and X. Q. Wang, *J. Phys. G* **29**, 2303 (2003), [arXiv:hep-ph/9910260].

- [40] T. Fuchs, J. Gegelia, G. Japaridze and S. Scherer, Phys. Rev. D **68**, 056005 (2003).
- [41] J. A. McGovern, Phys. Rev. C **63**, 064608 (2001) [Erratum-ibid. C **66**, 039902 (2002)].
- [42] S. R. Beane, M. Malheiro, J. A. McGovern, D. R. Phillips and U. van Kolck, Phys. Lett. B **567**, 200 (2003) [Erratum-ibid. B **607**, 320 (2005)]; Nucl. Phys. A **747**, 311 (2005).
- [43] V. Pascalutsa and D. R. Phillips, Phys. Rev. C **67**, 055202 (2003).
- [44] R. P. Hildebrandt, H. W. Griesshammer, T. R. Hemmert and B. Pasquini, Eur. Phys. J. A **20**, 293 (2004).
- [45] T. R. Hemmert, B. R. Holstein and J. Kambor, Phys. Rev. D **55**, 5598 (1997).
- [46] M. Schumacher, Eur. Phys. J. A **31**, 327 (2007).
- [47] A. I. L'vov, Phys. Lett. B **304**, 29 (1993).
- [48] B. R. Holstein, V. Pascalutsa and M. Vanderhaeghen, Phys. Rev. D **72**, 094014 (2005).
- [49] V. Pascalutsa, Prog. Part. Nucl. Phys. **55**, 23 (2005).
- [50] T. A. Gail and T. R. Hemmert, Eur. Phys. J. A **28**, 91 (2006).
- [51] V. Pascalutsa and M. Vanderhaeghen, Phys. Rev. Lett. **95**, 232001 (2005); Phys. Rev. D **73**, 034003 (2006).
- [52] L. S. Geng, J. Martin Camalich, L. Alvarez-Ruso and M. J. V. Vacas, Phys. Rev. Lett. **101**, 222002 (2008).
- [53] J. M. Camalich, L. Alvarez-Ruso, L. S. Geng and M. J. V. Vacas, arXiv:0904.4894 [hep-ph].
- [54] V. Lensky and V. Pascalutsa, JETP Lett. **89**, 108 (2009), [arXiv:0803.4115 [nucl-th]].
- [55] S. Weinberg, "The Quantum theory of fields. Vol. 2" (Cambridge U. P., 1996).
- [56] V. Pascalutsa, M. Vanderhaeghen and S. N. Yang, Phys. Rept. **437**, 125 (2007).
- [57] K. Johnson and E. C. Sudarshan, Annals Phys. **13**, 126 (1961).
- [58] G. Velo and D. Zwanziger, Phys. Rev. **186**, 1337 (1969).
- [59] F. Piccinini, G. Venturi and R. Zucchini, Lett. Nuovo Cim. **41**, 536 (1984).
- [60] V. Pascalutsa, Phys. Rev. D **58**, 096002 (1998).
- [61] V. Pascalutsa and R. G. E. Timmermans, Phys. Rev. C **60**, 042201 (1999).
- [62] V. Pascalutsa, Phys. Lett. B **503**, 85 (2001).
- [63] H. Krebs, E. Epelbaum and U. G. Meißner, arXiv:0812.0132 [hep-th]; arXiv:0905.2744 [hep-th].
- [64] A. Metz and D. Drechsel, Z. Phys. A **356**, 351 (1996).
- [65] J. Vermaseren, "Symbolic Manipulation with FORM," (Computer Algebra Nederland, Amsterdam, 1991).
- [66] T. Hahn and M. Rauch, Nucl. Phys. Proc. Suppl. **157**, 236 (2006).
- [67] F. E. Low, Phys. Rev. **96**, 1428 (1954); M. Gell-Mann and M. L. Goldberger, Phys. Rev. **96**, 1433 (1954).
- [68] B. Kubis and U. G. Meissner, Nucl. Phys. A **679**, 698 (2001).
- [69] V. Pascalutsa, B. R. Holstein and M. Vanderhaeghen, Phys. Lett. B **600**, 239 (2004).
- [70] D. Babusci, G. Giordano and G. Matone, Phys. Rev. C **57**, 291 (1998).
- [71] H. R. Weller *et al.*, Prog. Part. Nucl. Phys. **62**, 257 (2009); M. W. Ahmed, talk at INT Workshop "Soft Photons and Light Nuclei," Seattle, June 16 - 20, 2008.